A&A 368, 292–297 (2001)
DOI: 10.1051/0004-6361:20000545

Astronomy & Astrophysics

Comets in full sky L_α maps of the SWAN instrument

I. Survey from 1996 to 1998

J. T. T. Mäkinen[1], J.-L. Bertaux[2], T. I. Pulkkinen[1], W. Schmidt[1], E. Kyrölä[1], T. Summanen[1], E. Quémerais[2], and R. Lallement[2]

[1] Finnish Meteorological Institute, Geophysics Research, PO Box 503, 00101 Helsinki, Finland
[2] Service d'Aéronomie, BP 3, 91371 Verrières-le-Buisson, France

Received 29 September 2000 / Accepted 8 December 2000

Abstract. The SWAN instrument onboard the SOHO spacecraft is a Lyman α scanning photometer cabable of mapping the whole sky with 1° resolution. Since January 1996 the instrument has produced on average three full sky maps a week with the principal scientific objective of observing the distribution of heliospheric neutral hydrogen. In addition, these systematic observations are a valuable source for studying comets brighter than a visual magnitude of 7–11, the observing limit depending on the abundance ratios of produced radicals and the location of the comet relative to the galactic plane. When the data before the temporary loss of control of SOHO at the end of June 1998 were processed, altogether 18 comets were positively identified, of which one is a new discovery and another 5 can be detected on SWAN images before their actual discovery date. This demonstrates the feasibility of SWAN as an instrument for cometary surveys. The observations are used to estimate the water production rates of the detected comets near their perihelion passages.

Key words. data analysis – surveys – comets – ultraviolet: solar system

1. Introduction

The SOHO (Solar and Heliospheric Observatory) spacecraft has already been recognized as the most successful comet finder ever, the total number of discoveries exceeding 200 during less than five years of operation. Almost all new comets belong to the Kreutz sungrazer family and can be detected from LASCO (Large Angle and Spectrometric Coronagraph) images. While most of the SOHO instruments are studying the immediate surroundings of the Sun, one of them covers the rest of the sky. The SWAN (Solar Wind Anisotropies) instrument (Bertaux et al. 1995) onboard SOHO is a Lyman α multianode scanning photometer with an instantaneous field of view (FOV) of $5 \times 5°$ with 25 pixels $1 \times 1°$ each. The instrument consists of two sensor heads each of which has an overall FOV of over 2π steradians covering northern and southern ecliptic hemisphere, respectively. In the normal operation mode the instrument is capable of mapping the whole sky in one day but since the time has to be shared with other kinds of observations, the instrument has produced a complete sky map (Fig. 1) every three days on average. The observing activity has varied over the operational period (Fig. 2). In this respect the period from December 1996 to June 1998 represents the full capability of the instrument. At the end of the period the control of the spacecraft was lost for several months, and data gathered after the recovery show that the instrument was degraded through direct exposure to sunlight during the period of inactivity, decreasing its sensitivity and spectral resolution. Despite additional setbacks like the subsequent loss of attitude control gyroscopes of the spacecraft the observing campaign proceeds at full scale.

The primary use of the SWAN full sky UV maps is to study the latitudinal distribution of solar wind deductible from asymmetries in the cavity that it carves in the passing cloud of interstellar neutral hydrogen which resonantly scatters solar L_α light (Bertaux et al. 1999b). Another contribution to neutral hydrogen in the solar system comes from the photodissociation of H_2O, the major volatile component of cometary nuclei. Several known comets have been observed separately[1], obtaining valuable results (Bertaux et al. 1998, 1999a; Combi et al. 2000). Since these observations cannot create a complete track record of comets possibly detectable by the instrument, especially new comets only discovered near their

Send offprint requests to: T. Mäkinen,
e-mail: teemu.makinen@fmi.fi

[1] Besides most of the comets identified in this survey these include 69P/Taylor, 81P/Wild 2 and C/1997 J2 Meunier-Dupouy. Assessment of these data is still incomplete.

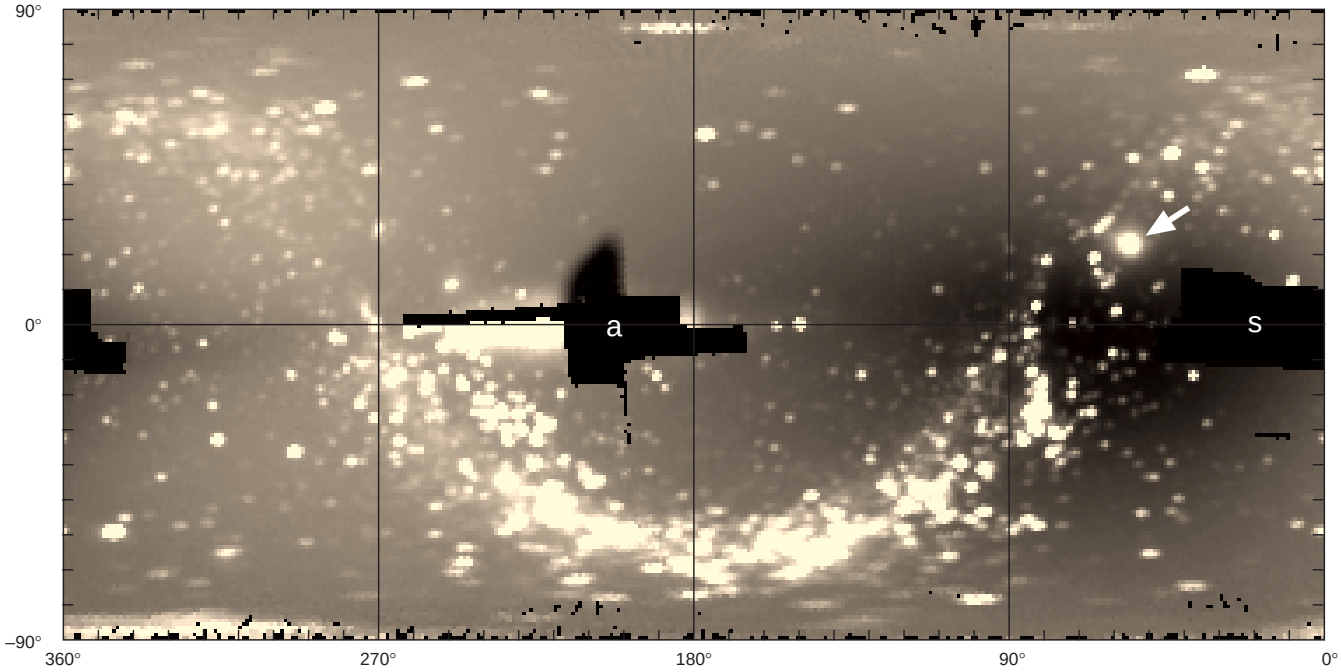

Fig. 1. SWAN full sky map in ecliptic coordinates. This 1° resolution UV image recorded April 9, 1996, shows the spatial distribution of interplanetary hydrogen, the area of bright stars near the galactic plane and the comet C/1996 B2 Hyakutake, denoted by the white arrow. The view of the instrument is always obstructed in two directions: pointing the instrument too close to the Sun (s) might damage the sensors, and the antisolar direction (a) is partly obstructed by the spacecraft itself. The locations of the unobservable zones change as the spacecraft moves on its orbit around the Sun

perihelion, a cometary survey was undertaken using the full sky images which constitute the most systematic set of measurements with best available coverage.

Since the SWAN instrument was not designed primarily to detect comets, its performance in this respect is far from ideal. The spatial resolution is restricted to the 1° of sensor pixels although this shortcoming is somewhat compensated by the fact that the hydrogen cloud of a comet is almost spherically symmetric and orders of magnitude larger than the visible dust tail. The point spread function (PSF) of the instrument has a standard deviation comparable to the pixel size near the L_α line but grows significantly towards the limits of the observing window of 115–170 nm and has a slight dependence on observing geometry. This spreads out the images of hot UV stars on the sky maps. The situation is further complicated by line of sight (LOS) retrieval inaccuracies which contribute another 1° of random diffusion to the observed signal. These effects together pose great difficulties for observing comets especially near the galactic plane where UV stars are abundant. Also the short exposure time of the normal mode – 13 s in any particular direction – gives only a modest signal to noise ratio despite the relatively high photometric sensitivity of about 0.84 counts per second per Rayleigh per pixel. All these complications are further accentuated on the post-recovery data but the systematic nature of observations combined with very high coverage and the location of the spacecraft at the L1 point between the Earth and the Sun, unpolluted by the Earth's exospheric L_α emission still makes the SWAN instrument an important tool for cometary studies.

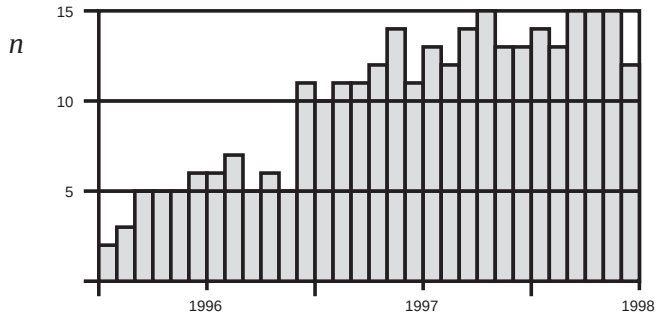

Fig. 2. Number of produced SWAN full sky maps per month from January 1996 to June 1998

2. Survey method

The aforementioned shortcomings in mind, a heuristic combined filtering and neural network method (Mäkinen et al. 2000b) was developed to detect all possible candidates for cometary objects. The single exposures of one observing session are binned into a $1 \times 1°$ grid in ecliptic coordinates. A variable-scale median difference filtering removes the smooth background caused by the interstellar neutral hydrogen cloud. The method is similar to the conventional overlaying of an image with its out-of-focus negative to reveal fine structure. The median filter was chosen

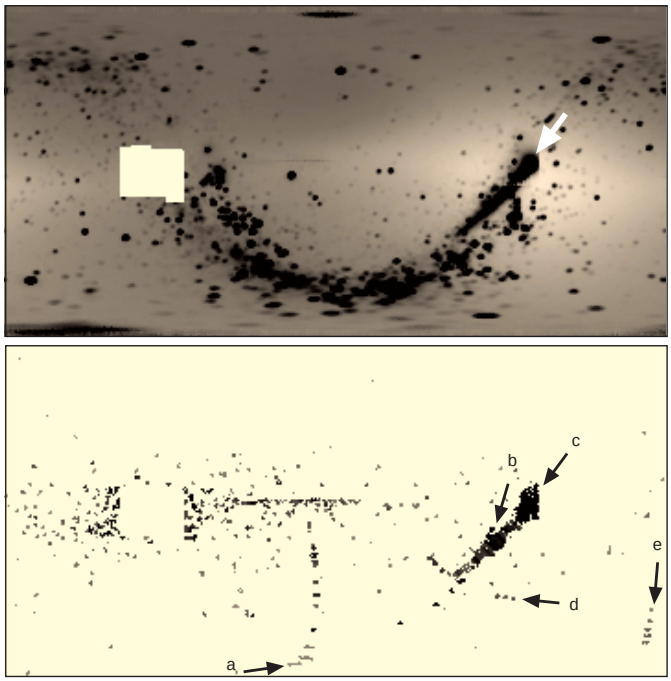

Fig. 3. Detecting comets with neural network. The trail of C/1995 O1 (Hale-Bopp) as denoted by the white arrow, is easily discernible on the combined sky image for the period of May to July 1997 (above). The neural network tracks minute differences in subsequent images and highlights the trails of other comets as well (below). Denoted by arrows are the trails of (a) C/1997 O1 (Tilbrook), (b) 2P/Encke, (c) C/1995 O1, (d) C/1997 N1 (Tabur) and (e) C/1997 K2. The random noise around the data gap is caused by reflections from the spacecraft

because it preserves sharp changes in base intensity, e.g., around the borders of a data gap. Since the remaining comets and stars appear identical in shape and because of the mentioned inaccuracies the random deformations of stars prevent direct image subtraction, a 3-layer bidirectional neural network was developed to process several months worth of images in a batch, highlighting consistent motion of any image feature. If S^k_{ij} is a set of T sky maps where the indices i and j denote longitude and latitude, respectively, and k the observing time, then the nodes in the successive layers A, B and C of the neural network are defined as

$$A^k_{ij} = \begin{cases} 1, & S^k_{ij} = \max\left[S^{\rm t}_{ij}\right] \\ 0 & \text{otherwise} \end{cases} \qquad k,t = [1,2,\ldots,T] \tag{1}$$

$$B^t_k = \begin{cases} 1, & b^{\rm t}_k \geq b_0 \\ 0 & \text{otherwise} \end{cases} \tag{2}$$

where $b^{\rm t}_k = \sum_{i,j} A^{\rm t}_{ij}$ over connected i, j and b_0 is a user-definable triggering threshold. The layer A and B node maps are thus two-dimensional and have one-to-one correspondence with the bins of the sky map. A layer A node fires when the corresponding bin receives its maximal value and a layer B node in the same location fires if the number of simultaneously firing adjacent layer A nodes exceeds the given threshold value. Then

$$\begin{aligned} C_{m_1\cdots m_T} = &\left[B^1_{k_{m_1}} + \cdots B^T_{k_{m_T}}\right] \\ &\times\text{median}\left[\; b^1_{k_{m_1}} g(i_{k_{m_1}}, j_{k_{m_1}}) + \cdots \right. \\ &\left. + \; b^T_{k_{m_T}} g(i_{k_{m_T}}, j_{k_{m_T}})\right] \end{aligned} \tag{3}$$

where the summation is over a particular trajectory and $g(i,j)$ is a geometric weight correction for spherical coordinates. The layer C nodes reside in the orbital parameters space and they are evaluated through initialization of potential traces of comets which are then followed over the layer B node map. The principle can be understood by visualizing an expanding and attenuating probability wave around every firing layer B node. Firing nodes are affected by the local probability field so that a nonlinear amplification of waves emitted by successive firings at suitable intervals soon forms a coherent pulse denoting the probable trajectory of a comet.

The implementation of the network contains several parameters for restricting the evaluation of layer C nodes shortening the processing time considerably. After the layer C is completed the data need to be visualized. Because the node space is multidimensional, the flow is reversed by feeding the obtained weights through established connections back to the layer A from which the results can be read. The output from the neural network (Fig. 3) depicts cometary trails which can be immediately compared to the orbits of known comets. The sensitivity of the neural network has been tested with simulated data and found to be comparable or in some cases even better than visual inspection of time lapse series of filtered images. The largest problem with the algorithm so far has been that the observation times are only known to an accuracy of one day but this problem could be eliminated by improving the data preprocessing tools.

3. Survey results

The SWAN images were processed by the neural network in quarterly sets. Altogether 18 comets as listed in Table 1 were identified from the SWAN full sky images from January 1996 to June 1998 of which C/1997 K2 proved to be a new discovery (Mäkinen et al. 2000a). The visibility period of every comet on SWAN images was determined by visually estimating the first and last images where the existence of a comet could be confirmed without a priori knowledge of its location. When the known orbital elements are used in combination with advanced processing methods these limits can be extended to yield valuable data. The list contains 6 short-period comets and 12 long-period comets. When the actual discovery dates of the long-period comets are compared to their visibility on SWAN it can be noticed that half of the long-period comets are visible on SWAN before their discovery. The situation is especially clear with comets C/1997 O1 (Tilbrook) and C/1998 J1 (SOHO) both of which were

Table 1. Comets found in SWAN full sky images. The table lists the perihelion time T_p and distance q, highest observed visual magnitude m_1, the visual magnitude of a comet when seen by SWAN the last time m_{1L} (where applicable), first and last positive detections of a comet and the total number N of sky images containing the comet

Comet	Name	T_p	q/[AU]	m_1	m_{1L}	Found	First	Last	N
2P	Encke	19970523.6	0.331	6	7.5		19970604	19970624	9
45P	Honda-Mrkos-Pajdusakova	19951226.0	0.532	7	7.1		19960128	19960202	2
46P	Wirtanen	19970314.2	1.064	10	10		19970125	19970313	20
55P	Tempel-Tuttle	19980228.1	0.977	8	10		19980101	19980324	38
96P	Machholz 1	19961015.1	0.125	4			19960928	19961012	4
103P	Hartley 2	19971222.0	1.032	8	10		19971115	19980217	42
C/1995 O1	Hale-Bopp	19970401.1	0.914	−2	4.7	19950723	19960706	19970920	142
C/1995 Y1	Hyakutake	19960224.3	1.055	8	8.7	19951225	19960202	19960313	6
C/1996 B1	Szczepanski	19960206.9	1.449	7	8	19960127	19960121	19960305	7
C/1996 B2	Hyakutake	19960501.4	0.230	−1	7.1	19960130	19960328	19960710	18
C/1996 N1	Brewington	19960803.4	0.926	8	9.2	19960704	19960706	19960918	16
C/1996 Q1	Tabur	19961103.5	0.840	5	9.7	19960819	19960918	19961110	11
C/1997 K2		19970626.2	1.546				19970520	19970718	24
C/1997 N1	Tabur	19970815.5	0.396	10		19970702	19970701	19970811	18
C/1997 O1	Tilbrook	19970713.4	1.372	10	11.0	19970722	19970520	19970826	41
C/1997 T1	Utsunomiya	19971210.1	1.359	10	10	19971003	19970919	19971223	43
C/1998 H1	Stonehouse	19980414.4	1.324	11	∼ 10.5	19980422	19980423	19980507	9
C/1998 J1	SOHO	19980508.6	0.153	0		19980503	19980224	19980623	59

found near the perihelion but the SWAN instrument has recorded months of prediscovery data.

The visual magnitude of a comet at the last time when it is detectable in SWAN images m_{1L} is given in Table 1 where it is relevant. From the listed values it can be estimated that the limiting magnitude for the SWAN instrument is 7–8 in areas of high star density and 10–11 in voids. Furthermore, the southern hemisphere sensor is less sensitive than the northern one by a factor of about 2.6 and this affects the detection limit. Considering these values, the early disappearance of C/1995 O1 (Hale-Bopp) is quite peculiar but it can be explained by the fact that at the moment the comet was located in a densely populated part of the galactic plane in the direction of Puppis and moving relatively little and it was, at least by visual observation, lost among background star contamination.

When the trails of the detected comets are depicted in the same plot (Fig. 4), it can be seen that the distribution is fairly homogeneous as a result of the high coverage of the SWAN instrument. When studying the list of known comets, it can be noticed that during the SWAN observing period two short-period comets, 22P/Kopff and 81P/Wild 2, were brighter than magnitude 11 for some time but nevertheless did not appear on the SWAN list of detected comets. It could be possible that the comets were relatively depleted in water thus making them that much dimmer in UV light but when one examines the orbits of these comets a more probable explanation can be seen. Both comets stay close to the ecliptic plane during the perihelion passage and once their locations are correlated with the SWAN visible area it can be noticed that both comets remain close to the part of the sky which is obstructed by the spacecraft. It can thus be concluded that the conducted survey is complete to the sensitivity limit of the instrument.

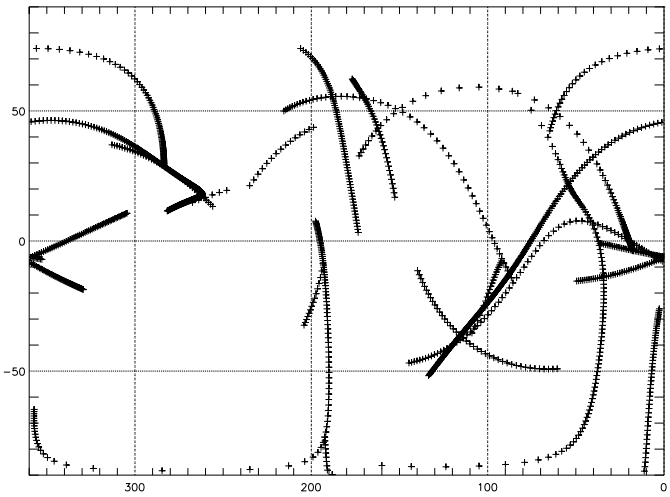

Fig. 4. Spatial coverage of all comets detected by SWAN. The trails of detected comets are plotted on ecliptic coordinates with one day stepping.

4. Water production rates for comets

The water production rate Q_{H_2O} of a comet is important because it is the most abundant product of cometary activity to which other production ratios are scaled. It can be derived from the observed neutral H distribution by assuming that the photodissociation of H_2O outside the collision sphere is the only noteworthy process. A simple stationary and monokinetic Haser model (Haser 1957; Festou 1981) is used to calculate the H column

densities for a reference value of $Q_{H_2O} = 1\ 10^{28}\ s^{-1}$. The equations follow directly from recursively applying the relation $dn(r) = (P(r) - \gamma n(r))\,dr$ for the density n where the production term $P(r)$ for daughter products is determined by the destruction rate of parent molecules. Thus for the $H_2O + h\nu \rightarrow OH + H_1$ reaction

$$N_1(r) = \frac{2Q_{H_2O}}{4\pi v_{H_1} r} \frac{\gamma_{H_2O}}{\gamma_{H_1} - \gamma_{H_2O}} \left[f(\gamma_{H_2O} r) - f(\gamma_{H_1} r) \right] \qquad (4)$$

and for the $OH + h\nu \rightarrow O + H_2$ reaction

$$N_2(r) = \frac{2Q_{H_2O}}{4\pi v_{H_2} r} \Big[\frac{\gamma_{H_2O}}{\gamma_{H_2} - \gamma_{H_2O}} \frac{\gamma_{OH}}{\gamma_{OH} - \gamma_{H_2O}} f(\gamma_{H_2O} r) - \frac{\gamma_{H_2O}}{\gamma_{OH} - \gamma_{H_2O}} \frac{\gamma_{OH}}{\gamma_{H_2} - \gamma_{OH}} f(\gamma_{OH} r) + \frac{\gamma_{H_2O}}{\gamma_{H_2} - \gamma_{H_2O}} \frac{\gamma_{OH}}{\gamma_{H_2} - \gamma_{OH}} f(\gamma_{H_2} r) \Big] \qquad (5)$$

where the subscripts denote hydrogen atoms produced in the first and second photodissociation, respectively, and the density is integrated over the entire column

$$f(q) = \int_0^{\pi/2} d\alpha \exp\left(-\frac{q}{\cos\alpha} \right) \qquad (6)$$

and γ_i and v_i are the inverse scale lengths and radial velocities of the respective particle populations[2] and r is the shortest distance between the column and the nucleus. The intensity map is then calculated taking into account the effect of the radial velocity of the comet on the L_α scattering efficiency and the spectral response of the instrument. The background contribution is eliminated by subtracting two observations from each other. The choice of observations is restricted by the conflicting requirements of sufficient separation between subsequent comet positions and minimal change in background signal possibly caused by variations in solar L_α intensity or by the stereoscopic effect of SOHO orbiting around the Sun. In practice most comets do not move rapidly enough for the observations to be considered independent and thus a simultaneous least squares fit of models for both the positive and negative image of the comet along with a second degree polynomial for background residual is calculated with the Singular Value Decomposition (SVD) method. Since the model is linear in Q_{H_2O} the fitting coefficients directly give the water production rates at both observations as well as an error estimation. For the purpose of this study, water production rate of each detected comet is calculated near the perihelion. The obtained values are listed in Table 2.

Table 2. Comet water production rates. Each comet is studied as close to perihelion as possible. The values for heliocentric r and geocentric Δ distance in AU and water production rate Q_{H_2O} of the comet are listed for the given date

Comet	Date	r	Δ	Q_{H_2O} 10^{28} s^{-1}
2P	970624	0.81	0.27	0.958
45P	960128	0.85	0.18	0.504
46P	970307	1.08	1.55	1.55
55P	980115	1.21	0.37	0.546
96P	961009	0.29	0.88	3.74
103P	971222	1.03	0.85	1.67
C/1995 O1	970401	0.91	1.34	1020
C/1995 Y1	960219	1.06	1.23	3.94
C/1996 B1	960202	1.45	0.74	1.88
C/1996 B2	960416	0.54	0.71	56.0
C/1996 N1	960807	0.93	0.90	0.774
C/1996 Q1	961015	0.92	0.47	4.22
C/1997 K2	970624	1.55	1.22	1.59
C/1997 N1	970710	0.97	1.17	0.913
C/1997 O1	970821	1.48	1.93	2.40
C/1997 T1	971206	1.36	1.86	3.86
C/1998 H1	980428	1.50	0.56	0.700
C/1998 J1	980516	0.32	0.88	71.4

5. Discussion

In the recent years the search for near-Earth objects (NEOs) has received considerable attention. The existing surveys, however, concentrate primarily on cataloguing all the potentially hazardous asteroids which is arguably a feasible objective since these objects are on orbits which bring them near enough to be observed every few years. The survey coverage is fairly limited which is demonstrated by the fact that amateurs still have a fair chance of discovering a new comet. Comets have much more variation in their orbital parameters and a large part of them may visit the inner solar system just once. Because of their higher kinetic energy and virtual invisibility before the nucleus is activated they pose a direct long term global threat. Collision probability estimates depend on the size distribution of comets which is still not adequately known.

The late discovery of C/1997 K2 and other prediscovery data underline the advantage of an instrument with full sky coverage in detecting new comets. An instrument looking for OH emission as suggested by Brandt et al. (1996a, 1996b) would not be affected by the interstellar neutral hydrogen. On the other hand this is not the largest problem in the SWAN data. The binning method applied in producing full sky maps contributes to the degradation of spatial resolution since it is optimized for large bin sizes. With advanced processing methods higher resolution will be achieved.

The use of the simple Haser model is justifiable in most situations. The largest comets provide ample data so that a more complex model can be used like with C/1995 O1 (Combi et al. 2000). Such models can also benefit from the rudimentary spectral measurement capacity of the instrument given by a H cell filter which can be used to derive the velocity of neutral H atoms. Full sky maps with H cell active are made as well although not as often as ordinary observations. Another shortcoming of the Haser model is apparent with comets whose Q_{H_2O} undergoes rapid fluctuations. A dynamical model could not use the

[2] The values used in this work were $1/\gamma_{H_2O} = 8.2\ 10^4$ km, $1/\gamma_{OH} = 2.25\ 10^5$ km, $1/\gamma_{H_1} = 3\ 10^7$ km, $1/\gamma_{H_2} = 1.2\ 10^7$ km, $v_{H_1} = 20$ km s^{-1} and $v_{H_2} = 8$ km s^{-1}

currently available full sky maps since their time resolution is too coarse. Thus, in combination with developing a time-dependent model one should use single exposures directly.

The SWAN full sky maps are very useful for calculating systematic water production rates with some caveats. Besides that the random spreading of stars on SWAN full sky maps introduces uncertainties to the determination of cometary water production rates, other sources of error exist which are not compensated for in this study. The spatial and temporal solar L_α intensity variations are considerable but in principle they could be tracked by observing the apparent background intensity changes at suitable areas over time. Furthermore, the instrument still has some calibration issues which must be addressed before a systematic record can be constructed. Especially the post-recovery data will need considerable calibrating effort. Once these issues have been adequately addressed, more comprehensive reviews can be produced concerning each major data set: the initial full sky observations, the post-recovery full sky observations and the comet specific observations.

Acknowledgements. SOHO is an international co-operative mission of ESA and NASA. SWAN was financed in France by CNES with support from CNRS and in Finland by TEKES and the Finnish Meteorological Institute. The work of J.T.T.M. and T.S. was supported by the Academy of Finland.

References

Bertaux, J. L., Kyrölä, E., Quémerais, E., et al. 1995, Solar Phys., 162, 403

Bertaux, J. L., Costa, J., Quémerais, E., et al. 1998, Planet. Space Sci., 46, 555

Bertaux, J. L., Costa, J., Mäkinen, T., et al. 1999a, Planet. Space Sci., 47, 725

Bertaux, J. L., Kyrölä, E., Quémerais, E., Lallement, R., et al. 1999b, Space Sci. Rev., 87, 129

Brandt, J. C., A'Hearn, M. F., Randall, C. E., et al. 1996a, Earth, Moon, & Planets, 72, 243

Brandt, J. C., A'Hearn, M. F., Randall, C. E., et al. 1996b, Small Comets (SCs): An Unstudied Population in the Solar System Inventory, in: Completing the Inventory of the Solar System, ed. T. W. Rettig, & J. M. Hahn, ASP Conf. Ser., 107, 289

Combi, M. R., Reinard, A. A., Bertaux, J. L., et al. 2000, Icarus, 144, 191

Festou, M. C. 1981, A&A, 95, 69

Haser, L. 1957, B. Acad. R. Sci. Liège, 43, 740

Mäkinen, J. T. T., Bertaux, J. L., Laakso, H., et al. 2000a, Nature, 405, 321

Mäkinen, J. T. T., Syrjäsuo, M. T., & Pulkkinen, T. I. 2000b, A method for detecting moving fuzzy objects from SWAN sky images, in Proceedings of the IASTED International Conference, Signal and Image Processing, November 19–23, 2000, Las Vegas, USA, 151